



Effects of alkali metal cations on oxygen reduction on N-containing carbons viewed as the interplay between capacitive and electrocatalytic properties: Experiment and theory

IGOR A. PAŠTI¹, ANA S. DOBROTA¹, NEMANJA M. GAVRILOV¹,
GORDANA ĆIRIĆ-MARJANOVIĆ^{1#} and SLAVKO V. MENTUS^{1,2*}

¹University of Belgrade – Faculty of Physical Chemistry, Studentski trg 12–16, 11158 Belgrade, Serbia and ²Serbian Academy of Sciences and Arts, Knez Mihajlova 35, 11000 Belgrade, Serbia

(Received 24 April, accepted 3 July 2019)

Abstract: The development of new electrocatalysts for the oxygen reduction reaction (ORR) is crucial for the sustainable energy economy. Both fundamental understanding of surface processes under operating conditions and suitable ORR activity measurements are necessary to select the best electrocatalyst candidate. In the present study, to contribute to this matter, we show that both the nature of alkali metal cations (Li^+ , Na^+ and K^+), composing supporting aqueous hydroxide solution, as well as the potential sweep rate in rotating disk electrode voltammetry measurements, influence the results of measurements of ORR activities of N-containing nanocarbons. Based on density functional theory calculations, we concluded that the specific interactions of hydrated cations with oxygen functional groups are responsible for such behaviour, leading to a close interplay between the electrode double layer charging and the parallel Faradaic process on carbon surface. From a practical point of view, the presented results indicate that it is necessary to standardize carefully the ORR measurements on different carbon materials.

Keywords: carbon electrocatalyst; ORR activity measurements; catalyst selectivity; double layer capacitance.

INTRODUCTION

Growing energy demands require quick finding of efficient ways to convert and store energy. In this sense, electrochemistry offers a variety of possible solutions, providing different types of power sources.¹ Most of the contemporary everyday needs are satisfied with batteries, but they are far from perfect solution. On the other hand, fuel cells (FCs) are complementary to batteries in terms of energy and power densities, but are inevitably connected with the use of catal-

* Corresponding author. E-mail: slavko@ffh.bg.ac.rs

Serbian Chemical Society member.

<https://doi.org/10.2298/JSC190426072P>

ysts. The particular problem connected with the FCs is the sluggish oxygen reduction reaction (ORR) which is the cathode reaction in different types of FCs.² So far platinum and its alloys are unbeaten in terms of ORR catalytic performance. Nevertheless, many reports so far witness the high catalytic activity of carbon materials, dominantly in alkaline media.^{3,4} If a carbon material is doped with nitrogen, boron or phosphorus (or any of their combinations), catalytic activity can be further improved.^{4,5}

Searching for novel efficient ORR catalyst requires proper catalyst testing and interpretation of obtained results. In the first step testing is done using rotating disk electrode (RDE) voltammetry, where the catalyst is deposited on the RDE surface in the form of a very thin film.⁶ In general, Pt and its alloys have rather rich surface electrochemistry and the catalytic activity has been linked with surface processes taking place under operating conditions.⁷ However, it is now widely accepted that the experimental conditions, like the potential scan rate in RDE voltammetry experiments, affects the measured catalytic activities, which was shown for both polycrystalline Pt⁸ and Pt/C catalysts.⁹ Hence, a lot of effort was invested to standardize the procedures for assessment of electrocatalytic activity of Pt-based catalysts, including both polycrystalline Pt and carbon-supported nanosized Pt.^{10,11}

Another fundamental aspect related to catalyst testing would be the effect of the “inert” (supporting) electrolyte on the catalytic activity. When looking at standard textbooks in electrochemistry, inert electrolyte has many crucial roles, but it is essentially considered as a phase which contains electroactive species. Its effect on the electrochemical process itself should not be present, excluding the effects of pH, specific adsorption and the cases where concentration of inert electrolyte is low so that the effect of electrical double layer (EDL) structure is seen.¹² In practice, this is not the case. Over the years a significant number of results have been accumulated showing a substantial effect of the inert electrolyte on the electrochemical processes, although there are no electrochemical reactions in which inert electrolyte is directly involved. When considering catalytic activity, maybe the best known example is the work of Marković group,¹³ which demonstrated the effect of alkali metal cation (M^+) from MOH aqueous solution on the catalytic activity of Pt(111) surface. When ORR is considered, the activity of Pt(111) surface increases in the following order: LiOH < NaOH < KOH < CsOH.¹³ These effects were ascribed to the formation of $\text{OH}_{\text{ads}}-\text{M}^+(\text{H}_2\text{O})_n$ cluster on Pt surface, which block the active sites for ORR and reduce the catalytic activity as the hydration sphere of M^+ increases.¹³ Quite recently the same topic was investigated by Bondarenka group,¹⁴ who extended their investigation to the effects of alkali metal cations on hydrogen evolution reaction (HER) as well.¹⁵ There are two interesting points to outline here. First, the effect of alkali metal cations is opposite for ORR and HER on Pt (and also depends on the metal which

is used as the electrocatalyst), and second, the effect is seen in a wide potential window, at positive potentials corresponding to ORR and negative potentials corresponding to HER. When looking at carbon materials, just recently it was demonstrated that alkali metal and earth alkaline metal cations have striking effect on the process of electrochemical reduction of graphene-oxide.¹⁶ This process takes place at potentials where cations from supporting electrolyte cannot be reduced, so the effect was ascribed to the interaction of M^+ and M^{2+} with oxygen functional groups, resulting with their activation towards the reduction process. Hence, one might expect that the effect of alkali metal cations from supporting electrolyte could be expected in some other cases, like ORR.

Some time ago, our group observed the effect of the potential scan rate on the ORR activity of polymer-derived N-containing carbon materials, which was ascribed to the specific interactions of ions from the solution with nitrogen moieties in the materials' structure.¹⁷ Such conclusion was motivated by the analogous effect of the potential scan rate on the capacitive response, essentially linking lower state of charge of EDL with higher catalytic activity. In essence, the effect was the same as in the case of Pt-based materials. Higher scan rate resulted with higher measured ORR activity, but the underlying mechanisms were different. Namely, in the case of Pt it is due to the place exchange process on partially oxidized surface.⁸ This essentially means that capacitive and Faradaic processes are not independent and that the former affect the latter ones. In this work we analyze the effects of the potential scan rate in RDE voltammetry measurements of ORR activities of N-containing carbon materials and combine them with the effects of the "inert" electrolyte by providing the measurements in LiOH, NaOH and KOH aqueous solutions. For this study we selected the previously used N-containing polyaniline (PANI) derived carbons, denoted as C-PANI-SSA and C-PANI-DNSA, produced by the carbonization of PANI doped with 5-sulfosalicylic acid (SSA) and 3,5-dinitrosalicylic acid (DNSA), as described in details in literature.^{17,18} The obtained results point to a necessity of standardization of ORR measurements on carbon materials, which might be much more demanding than in the case of Pt-based catalysts.

EXPERIMENTAL

Electrochemical measurements

The N-containing carbon catalysts were prepared by dispersing 4.0 mg of C-PANI-SSA or C-PANI-DNSA sample in 1 cm³ of ethanol/water mixture (40 vol.% of ethanol). The suspension was homogenized in an ultrasonic bath for 30 min. The suspension was drop-casted onto the surface of glassy carbon (GC) rotating disk electrode (geometrical cross-section area 0.196 cm²) and dried under N₂ stream. After the catalyst layer was dried, it was covered with 10 µL of 0.05 wt.% solution of Nafion in ethanol. The solvent was removed by evaporation. The loading of carbon catalyst on the electrode was set to 200 µg cm⁻². Thus the obtained electrode was tested by cyclic voltammetry (CV) in selected aqueous electrolytic solution (0.1 mol dm⁻³ LiOH, NaOH or KOH; Sigma Aldrich, ACS grade) purged by nitrogen stream, to

investigate its capacitive response, or by RDE voltammetry in O₂-saturated solution, to investigate its ORR electrocatalytic properties. The electrochemical measurements were done in a conventional one-compartment three-electrode electrochemical cell, with graphite rod as a counter electrode and a saturated calomel electrode (SCE) as a reference electrode. High purity N₂ and O₂ (99.995 %, Messer, Serbia) were used for these experiments. The measurements were done at room temperature using Gamry PCI4/750 potentiostat/galvanostat equipped with PINE rotator.

Theoretical calculations

Periodic DFT calculations were performed within the generalized gradient approximation (GGA) using Perdew–Burke–Ernzerhof (PBE) parametrization of exchange correlation functional.¹⁹ All the calculations were spin-polarized and carried out using PWscf code of Quantum Espresso,²⁰ which incorporates ultra-soft pseudopotentials and plane wave basis set. The plane waves' kinetic energy cut-off was 36 Ry while the charge density cut-off was 576 Ry. The graphene surface were modelled as one layer consisted out of 24 atoms arranged in a honeycomb lattice, which corresponds to the (2 $\sqrt{3}$ ×2 $\sqrt{3}$)R30° structure, following previous reports.²¹ N-doping was modelled by substituting one C atom with nitrogen, resulting with the nitrogen concentration of about 4.17 at.%. To model the oxidized surface of (doped) graphene one epoxy group was introduced on the surface, resulting with the same concentration of N and O (finally 4 at.% for both O and N). The position of epoxy group on the N-doped surface was located previously.²² The *k*-point sampling was 4×4×1, generated using the scheme of Monkhorst and Pack.²³ The atomic positions were fully relaxed until the remaining forces on atoms were below 0.002 eV Å⁻¹. The calculations were performed with correction for the long range dispersion interactions using the DFT-D2 scheme of Grimme.²⁴ The interaction of alkali metal atoms (Li, Na and K) with the investigated graphene surfaces was quantified in terms of adsorption energies (E_{ads}) calculated as:

$$E_{\text{ads}} = E_{\text{M+S}} - (E_{\text{S}} + E_{\text{M}}) \quad (1)$$

where $E_{\text{S+M}}$, E_{S} and E_{M} stand for the total energy of O-functionalized graphene model surface (N-graphene, epoxy-graphene or N-epoxy-graphene) with alkali metal M, the total energy of a given model surface and the total energy of isolated M atom, respectively. Charge redistribution caused by alkali metal interaction with the modified graphene surfaces was visualized using 3D plots of charge density difference ($\Delta\rho$), defined as:

$$\Delta\rho = \rho_{\text{S+M}} - \rho_{\text{S,frozen}} - \rho_{\text{M}} \quad (2)$$

where $\rho_{\text{S+M}}$, $\rho_{\text{S,frozen}}$ and ρ_{M} represent the ground state charge densities of the substrate interacting with M, the frozen substrate when the adsorbate is removed, and of the isolated adsorbate in the configuration corresponding to adsorption, respectively.

RESULTS AND DISCUSSION

Selected PANI-derived carbons, C-PANI-SSA and C-PANI-DNSA, have the similar morphology dominated by 1D nanostructures (nanorods, accompanied with nanotubes in the case of C-PANI-SSA) but they differ in nitrogen and oxygen content and their textural properties.^{17,18} The main relevant characteristics are outlined in Table I.

The cyclic voltammograms of both C-PANI-DNSA (Fig. 1) and C-PANI-SSA (Fig. 2) do not have rectangular shape characteristic for ideal capacitive behaviour, moreover their current response is much more pronounced at negative

TABLE I. Properties of carbon materials used in this work¹⁷

Property	C-PANI-SSA	C-PANI-DNSA
N content ^a , at.%	7.0	5.5
O content ^a , at.%	4.6	7.0
Specific surface area ^b , m ² g ⁻¹	317	441
$V_{\text{micro}}/(V_{\text{micro}} + V_{\text{meso}})^c$	62.7	90.2

^aDetermined by XPS; ^bBET surface area; ^cfraction of micropores in total pore volume (excluding macropores)

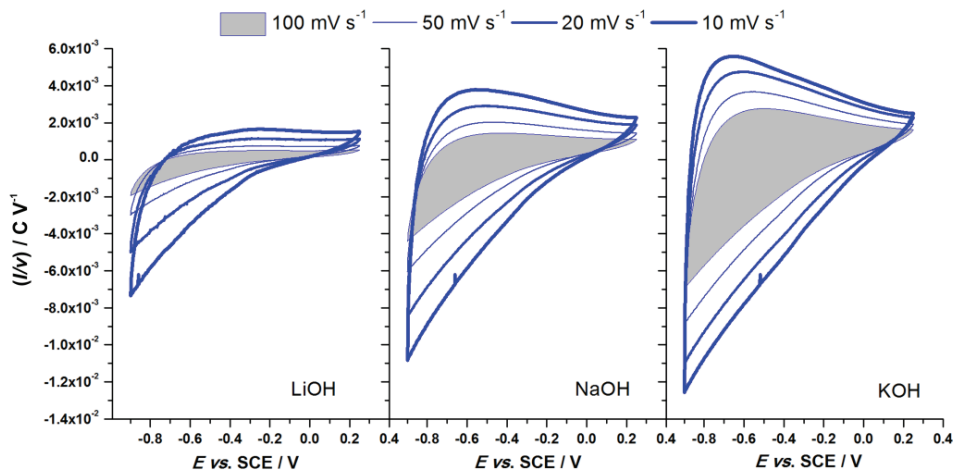


Fig. 1. Cyclic voltammograms of C-PANI-DNSA in 0.1 mol dm⁻³ aqueous solutions of LiOH (left), NaOH (middle) and KOH (right). Cyclic voltammograms are normalized by potential scan rate.

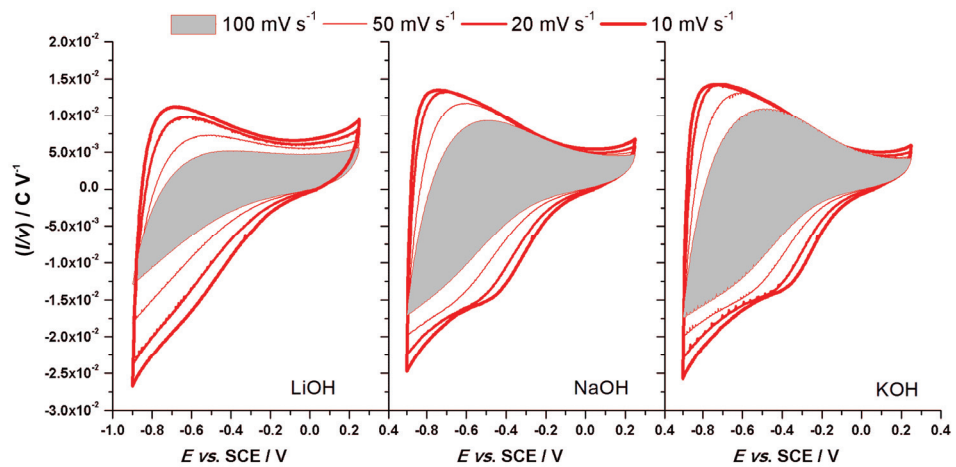


Fig. 2. Cyclic voltammograms of C-PANI-SSA in 0.1 mol dm⁻³ aqueous solutions of LiOH (left), NaOH (middle) and KOH (right). Cyclic voltammograms are normalized by potential scan rate.

potentials (*i.e.* below -0.2 V *vs.* SCE). We ascribe this behaviour to pseudocapacitance associated with the presence of nitrogen and oxygen functional groups on their surface, which is triggered at negative potentials, while double layer capacitance is dominant at higher potentials. The provided cyclic voltammograms are normalized by the potential sweep rate, giving in fact differential capacitance. There are two general features which have to be outlined. First, the capacitance is significantly higher when the potential sweep rate is lower, and, second, the capacitive response increases from LiOH to NaOH and becomes the highest in KOH solution. The same effect was also observed in the case of graphene with a small fraction of oxygen functional groups, and explained by the specific interactions of alkali metal cations from the solution with these surface functional groups.²⁵ Considering the contribution of pseudocapacitance, in the case of C-PANI-DNSA voltammograms are rather featureless, but in the case of C-PANI-SSA their shape, particularly in the low potential region, clearly indicates the presence of pseudocapacitance. Moreover, the capacitive response of C-PANI-SSA is 2-3 times higher than that of C-PANI-DNSA, in agreement with previous capacitance measurements.¹⁸

We confirmed that the (pseudo)capacitive response of the investigated carbons is not influenced by the diffusion from the solution (by RDE experiments in blank solutions) and ascribed very different capacitive behaviour of C-PANI-DNSA and C-PANI-SSA primarily to the differences in their textural properties. C-PANI-DNSA is dominantly microporous (Table I) and diffusion in micropores is slower for more hydrated ions ($\text{Li}^+ > \text{Na}^+ > \text{K}^+$). In contrast, C-PANI-SSA has much more opened structure with higher contribution of mesopores (Table I) and the capacitive response at low potential sweep rates is quite similar in all three electrolytes (Fig. 2). However, the capacitance decays from KOH to LiOH as in the case of C-PANI-DNSA.

ORR RDE polarization curves for C-PANI-DNSA (Fig. 3) and C-PANI-SSA (Fig. 4) show that both composition of supporting electrolyte and the potential scan rate affect the measured ORR activity.

When considering ORR currents recorded for C-PANI-DNSA at 10 mV s^{-1} (Fig. 3, left), we see that ORR onset potential is almost unaffected by the electrolyte, but the differences are more pronounced in the mixed kinetics region. This coincides with the potential window where the capacitive response is the most sensitive to the potential scan rate and where the significant differences in the EDL state of charge arise for potential sweeps at different rates. In general, the current response in LiOH solution is smaller than in the cases of NaOH and KOH solutions, the latter two cases being quite similar. When ORR is measured at higher potential sweep rate (50 mV s^{-1} , Fig. 3 right), more pronounced differences are seen in the kinetically controlled region, and the onset potential is shifted to more positive potential, compared to that observed at 10 mV s^{-1} . Following

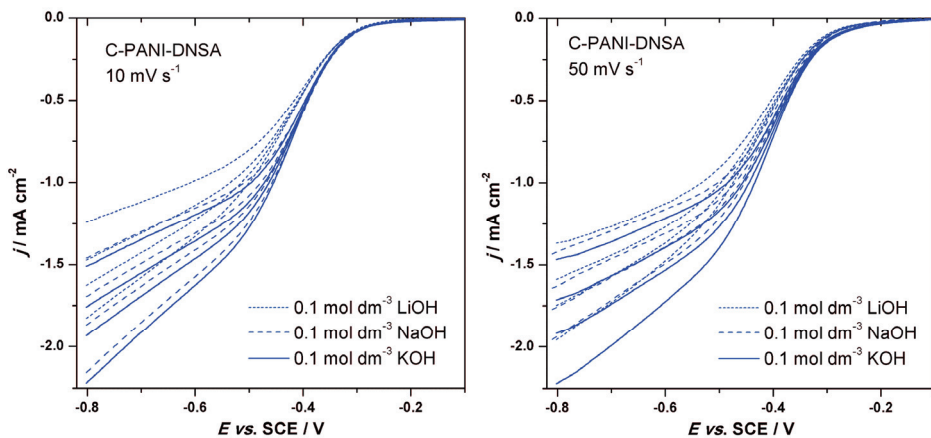


Fig. 3. Background-corrected RDE voltammograms of C-PANI-DNSA in O_2 -saturated 0.1 mol dm^{-3} aqueous solutions of LiOH (dotted), NaOH (dashed) and KOH (solid), recorded at different electrode rotation rates (600, 900, 1200 and 1800 rpm). RDE curves are given for two potential scan rates: 10 (left) and 50 mV s^{-1} (right).

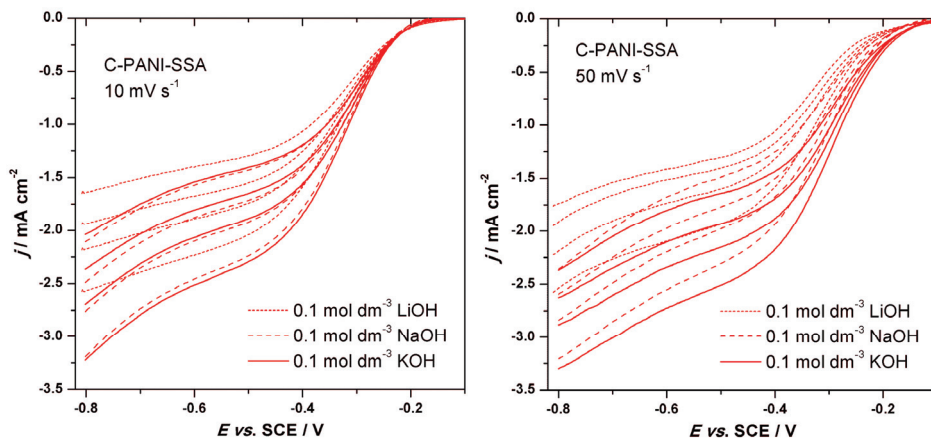


Fig. 4. Background-corrected RDE voltammograms of C-PANI-SSA in O_2 -saturated 0.1 mol dm^{-3} aqueous solutions of LiOH (dotted), NaOH (dashed) and KOH (solid), recorded at different electrode rotation rates (600, 900, 1200 and 1800 rpm). RDE curves are given for two potential scan rates: 10 (left) and 50 mV s^{-1} (right).

the practice to compare ORR activities on the basis of the onset potential, an immediate conclusion would be that the material is more catalytically active when measured at higher sweep rate. Considering the differences in a capacitive response, higher catalytic activity could be correlated with a lower state of charge at higher potential sweep rates. Hence, one might consider ions forming the EDL as spectator species, like OH_{ads} for the case of Pt and Pt-based ORR electrocatalysts.⁷ As previously observed,¹⁷ we see that C-PANI-SSA is more active than

C-PANI-DNSA, both in terms of ORR onset potential and the current response in kinetically controlled region and the mixed kinetics region (Fig. 4). At low scan rate the behaviour is qualitatively similar to that of C-PANI-DNSA, but at 50 mV s⁻¹ (Fig. 4, right) the behaviour is much different. An extreme effect of the supporting electrolyte is seen and the current response is affected by diffusion of O₂ even at very low ORR overpotentials. However, we again see that the highest activity is observed when measured in KOH, followed by NaOH and LiOH supporting electrolyte solution.

We note that on both materials ORR is not under full diffusion control, and rather constant rise in ORR current is seen with the increase of cathodic polarization. We have previously shown that ORR on carbon materials is highly influenced by the catalyst loading,¹⁷ but achieving the full diffusion control might result with such a high mass of the catalyst on the RDE surface that the necessary conditions for a well defined RDE experiments might be violated. Nevertheless, the variations in the current response in mixed kinetics region are a clear indication that the selectivity of carbon catalyst might also be influenced by the polarization scan rate and the supporting electrolyte composition. Hence, the ORR polarization curves were subjected to Koutecky–Levich (K–L) analysis,²⁶ in order to determine the apparent number of electrons consumed per O₂ molecule (*n*), *i.e.*, the catalyst selectivity. The apparent number of electrons is determined from the slope of K–L lines defined by:

$$\frac{1}{j(E)} = \frac{1}{j_k(E)} + \frac{1}{j_d} = \frac{1}{j_k} - \frac{1}{0.62nFD(O_2)^{2/3}\nu^{-1/6}\omega^{1/2}c(O_2)} \quad (3)$$

In Eq. (3), $j(E)$ and $j_k(E)$ are the measured current density and the kinetic current density at a given electrode potential (*E*), respectively, while j_d is the limiting diffusion current density (which indirectly depends on *E* via *n*). Furthermore, ν presents the kinematic viscosity of the solution (0.01 cm² s⁻¹)²⁷, $D(O_2)$ is the diffusion coefficient of O₂ (1.9×10⁻⁵ cm² s⁻¹)²⁸ and $c(O_2)$ is the concentration of dissolved O₂ (1.2×10⁻⁶ mol cm⁻³).²⁸ The provided constants are given for KOH solution and any variation could lead to different j_d in supporting electrolytes used here. However, we note that according to Strmcnik *et al.*¹³ the limiting diffusion current in LiOH, NaOH and KOH are rather similar (within approx. 5 %) as it was observed that ORR is under the full diffusion control on Pt(111), insensitive to the supporting electrolyte (in the range of alkali metal hydroxides). Hence, we used the constants for 0.1 mol dm⁻³ KOH solutions to evaluate *n* for all three electrolytes. The catalyst selectivity towards O₂ reduction to OH⁻ is given in Fig. 5 (evaluated at -0.7 V vs. SCE). The results indicate the behaviour which is expected from RDE polarization curves – with a few exceptions, *n* increases with the potential sweep rate and decreases from KOH to NaOH and, finally, LiOH.

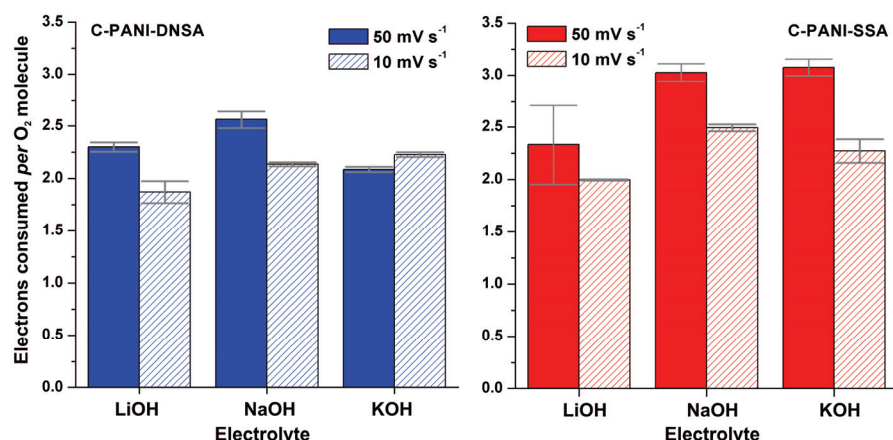


Fig. 5. Evaluated number of electrons consumed per O_2 molecule (at -0.7 V vs. SCE) for C-PANI-DNSA (left) and C-PANI-SSA (right) with two potential scan rates (10 and 50 $mV\ s^{-1}$).

It is important to note that the number of electrons consumed per O_2 is between 2 and 4, but, generally, we consider that ORR actually proceeds via $2e^-$ reduction to peroxide (HO_2^-). Thus formed HO_2^- goes further into the chemical disproportionation to OH^- and O_2 . When O_2 is formed in this chemical step it enters the next electrochemical reduction effectively increasing n above 2.²⁹ Based on this mechanism, the overall differences in ORR activities and selectivities of C-PANI-SSA and C-PANI-DNSA can be understood through the difference in textural properties/porosity. In the case of C-PANI-DNSA only the active sites at external surface could contribute to the activity, while in the case of C-PANI-SSA mesopores could also provide active sites for ORR. However, this cannot explain more delicate effects observed here.

Considering the effect of the potential scan rate, the results reported here agree with our previous results, where only KOH was used as the supporting electrolyte.¹⁷ While the observed effects were previously ascribed to the interactions of M^+ with N moieties in carbons, based on literature,³⁰ we re-examined this explanation by DFT calculations. For this purpose, the interactions of alkali metal atoms were investigated with N(-O)-modified graphene surfaces (Fig. 6).

While there is a difference between interactions of metal atoms and metal ions with surfaces (through the presence of hydration shells) we noted that everything was correct with the electron count in the system. In our calculations electron comes from alkali metal atom valence shell and in an electrochemical system it comes from outer electronic circuit, finally giving a charge-neutral system. From the charge density maps it can be seen that this electron dominantly settles on carbon surface around the N(-O) defect and the defect itself. The obtained results (Fig. 6) show that the direct interactions with N in graphene surface is

energetically inferior compared to the interactions with oxygen functional groups, epoxide in this particular case. However, if N-dopant is present (as in the case of C-PANI-SSA and C-PANI-DNSA) at the surface, it further boosts the interactions of M with epoxide, in agreement with previous observations.²² We note that it was observed previously that O-functional groups tend to aggregate around defects on carbon surface,²¹ so this scenario could be generally applicable. Hence, the above given hypothesis might be only partially true – the interaction of alkali metal cations with the carbon surface is influenced by nitrogen incorporated in the structure, but indirectly, through the effect of nitrogen on the oxygen functional groups. The electron localization observed on the charge difference maps is considered as the origin of pseudocapacitance observed in voltammetric experiments (Figs. 1 and 2).

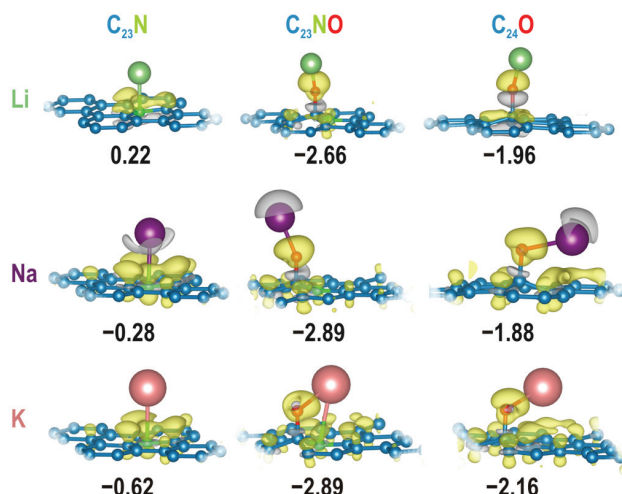
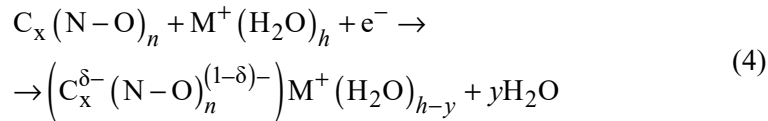


Fig. 6. Li, Na and K interacting with graphitic N in graphene surface (left column), N-epoxy moiety (middle) and epoxy-group on graphene surface (right). Numbers below the structures give M adsorption energies (eV atom^{-1}) according to Eq. (1). Isosurfaces of charge density are provided to observe bond formation upon adsorption of metal atom.

In order to correlate the theoretical calculations with the experimentally observed behaviour we compare hydration energies of Li^+ , Na^+ and K^+ with calculated adsorption energies (Fig. 6). In the series of alkali metal cations hydration energies increase from -520 (Li^+) to -410 kJ mol^{-1} (Na^+) and -320 kJ mol^{-1} (K^+). This means that in the case of Li^+ the adsorption energy of Li on N(–O) moieties the fraction hydration energy is smaller than in the case of Na and K, meaning that the hydration spheres of Li^+ can be less disrupted than in the case of Na^+ and particularly K^+ . This leads to the conclusion that (hydrated) Li^+ is located at larger distances from carbon surface than Na^+ and K^+ , whose hydration

spheres can be partially disrupted at the expense of the interactions with surface functional groups, following general reaction:



In the equation above, C_x is the fraction of graphene basal plane in the vicinity of N–O moieties and h is the number of H_2O molecules in the hydration shell of M^+ . Extra electron brought to the system localizes at the N–O moiety and at the part of the graphene basal plane, according to Fig. 6. The process described by Eq. (4) brings outer Helmholtz plane closer to the carbon surface. As smaller charge separation distances results with higher capacitance values, this additionally supports the difference in (pseudo)capacitive responses when switching from LiOH to NaOH and KOH, as experimentally observed. Now, there is an apparent discrepancy regarding the correlation between EDL state of charge and the ORR catalytic activity. Namely, if three different electrolytes are considered (keeping the potential sweep constant), then lower state of charge (the lower capacitance) results with lower ORR activity. If potential sweep rate effect is considered (in one electrolyte) than lower state of charge corresponds to higher ORR activity. We consider that both effects can be explained by the steric hindrance caused by hydrated alkali metal cations at N–O-containing carbon surface. If the effect of electrolyte is considered, then ORR is more hindered by larger hydrated Li^+ , while in the case of Na^+ and K^+ the O_2 molecule can penetrate through the layer of hydrated ions, whose hydration shell are partially disrupted *via* interactions with the surface functional groups according to Eq. (4). If the effect of the scan rate is considered the variation of activity, it can be understood through a smaller number of ions electrosorbed at the interface when potential sweep is faster (Figs. 1 and 2). In both cases we considered that there was a strong interplay between capacitive and Faradaic processes at the interface, two types of processes that are traditionally considered as independent and parallel to each other. This assumption is deeply incorporated in the procedures for testing ORR catalytic activity as capacitive response recorded in the absence of O_2 is considered as background.

Besides the fundamental aspect related to the interplay between EDL charging and electrocatalytic processes on the carbon surface, we noted that from the practical point of view presented the results indicated that it is necessary to carefully standardize measurements of ORR activity on carbon materials. However, an additional problem is related to the inherent presence of oxygen-containing groups on virtually any carbon surface. While the concentration and type of O-functional groups can differ greatly from one sample to another, the main problem is that we do not know what happens to them under electrochemical con-

ditions and, as a rule, it is commonly considered that the groups on carbon surface *in situ* are identical to the ones identified *ex situ* (which often required vacuum conditions like in XPS). This is in contrast to the case of Pt-based catalyst where the presence and the concentration (that is the coverage) of O-surface groups is potential-dependent and can be controlled relatively easily. However, if one intends to use carbon as a FC catalyst, the most appropriate way to test the catalyst might be RDE chronoamperometry, as it provides information for both transient conditions (during EDL charging) and stationary conditions (as in operating FC). Moreover, due to the effect of catalyst loading on the ORR activity, the used loading should be reported precisely and/or ORR activity should be measured for several catalyst loadings.

CONCLUSION

We have demonstrated that both the composition (*i.e.*, cation nature) of the supporting (inert) electrolyte and the potential sweep rate in the RDE voltammetry affect the measured ORR activities of N-containing nanocarbons. In general, the measured currents in the kinetic and the mixed control regions and ORR onset potentials are lower when the alkali metal cation from the electrolyte is more hydrated ($\text{Li}^+ > \text{Na}^+ > \text{K}^+$) and when the potential sweep is slower. The DFT calculations show that the interactions of hydrated M^+ with the oxygen functional groups could explain the effect of the supporting electrolyte and the potential sweep rate on the capacitive properties, which are deeply correlated with the ORR process on carbon surface. In overall, we conclude that the ORR (Faradaic process) must not be considered separately from both the EDL charging and the pseudocapacitive processes on carbon catalyst surface. The presented results also invoke the conclusion that it is necessary to standardize ORR measurements on carbon catalysts, as the experimental conditions could greatly affect the estimated ORR activity and the selectivity of studied carbon catalyst.

Acknowledgments. This work is dedicated to Professor Miljenko Perić on the occasion of his 70th birthday. Authors acknowledge the support provided by the Serbian Ministry of Education Science, and Technological Development (Grants No. III45014 and OI172043), and by the Serbian Academy of Sciences and Arts, project F-190.

ИЗВОД

ЕФЕКАТ КАТЈОНА АЛКАЛНИХ МЕТАЛА НА РЕАКЦИЈУ РЕДУКЦИЈЕ КИСЕОНИКА НА УГЉЕНИЦИМА КОЈИ САДРЖЕ АЗОТ У СВЕТЛУ ПОВЕЗАНОСТИ КАПАЦИТИВНИХ И ЕЛЕКТРОКАТАЛИТИЧКИХ СВОЈСТАВА – ЕКСПЕРИМЕНТ И ТЕОРИЈА

ИГОР А. ПАШТИ¹, АНА С. ДОБРОТА¹, НЕМАЊА М. ГАВРИЛОВ¹, ГОРДАНА ЂИРИЋ-МАРЈАНОВИЋ¹
и СЛАВКО В. МЕНТУС^{1,2}

¹Универзитет у Београду – Факултет за физичку хемију, Студентски бр 12-16, 11158 Београд и
²Српска академија наука и уметности, Кнез Михајлова 35, 11000 Београд

Развој нових електрокатализатора за реакцију редукције кисеоника (РРК) је кључан за одрживи енергетски развој. За избор најбољег кандидата неопходна су основна схва-

тња површинских процеса под радним условима као и одговарајућа мерења активности према РРК. Да би се допринело овом питању, у овој студији, показано је да природа катјона алкалних метала (Li^+ , Na^+ и K^+), који потичу из воденог раствора хидроксида коришћеног као основни електролит, као и брзину скенирања потенцијала у волтаметријским мерењима са ротирајућом диску електродом, утичу на резултате мерења активности према РРК на угљеницима допираним азотом. На основу израчунавања базираних на теорији функционала густине, закључено је да су специфичне интеракције хидратисаних катјона са кисеоничним функционалним групама одговорне за уочено понашање. Ово наводи на закључак да су капацитивни процеси пуњења двојног електричног слоја и паралелни фарадејски процеси на површини угљеника међусобно повезани. Са практичне тачке гледишта, представљени резултати указују да је потребно пажљиво стандардизовати мерења РРК на различитим угљеничним материјалима.

(Примљено 24. априла, прихваћено 3. јула 2019)

REFERENCES

1. M. Winter, R. J. Brodd, *Chem. Rev.* **104** (2004) 4245 (<https://doi.org/10.1021/cr020730k>)
2. N. M. Markovic, P. N. Ross, *Surf. Sci. Rep.* **45** (2002) 117 ([https://doi.org/10.1016/S0167-5729\(01\)00022-X](https://doi.org/10.1016/S0167-5729(01)00022-X))
3. K. Gong, F. Du, Z. Xia, M. Durstock, L. Dai, *Science* **323** (2009) 760 (<https://doi.org/10.1126/science.1168049>)
4. I. A. Pašti, A. J. Ležaić, N. M. Gavrilov, G. Ćirić-Marjanović, S. V. Mentus, *Synth. Met.* **246** (2018) 267 (<https://doi.org/10.1016/j.synthmet.2018.11.003>)
5. I. A. Pašti, N. M. Gavrilov, A. S. Dobrota, M. Momčilović, M. Stojmenović, A. Topalov, D. M. Stanković, B. Babić, G. Ćirić-Marjanović, S. V. Mentus, *Electrocatal.* **6** (2015) 498 (<https://doi.org/10.1007/s12678-015-0271-0>)
6. G. Chen, M. Li, K. A. Kuttiyiel, K. Sasaki, F. Kong, C. Du, Y. Gao, G. Yin, R. R. Adzic, *Electrocatal.* **7** (2016) 305 (<https://doi.org/10.1007/s12678-016-0309-y>)
7. V. R. Stamenkovic, B. Fowler, B. S. Mun, G. Wang, P. N. Ross, C. A. Lucas, N. M. Marković, *Science* **315** (2007) 493 (<http://doi.org/10.1126/science.1135941>)
8. I. A. Pasti, N. M. Gavrilov, S. V. Mentus, *Int. J. Electrochem. Sci.* **7** (2012) 11076 (<http://www.electrochemsci.org/papers/vol7/71111076.pdf>)
9. N. Hodnik, C. Baldizzone, S. Cherevko, A. Zeradjanin, K. J. J. Mayrhofer, *Electrocatal.* **6** (2015) 237 (<https://doi.org/10.1007/s12678-015-0255-0>)
10. S. Mentus, I. Pasti, *IPSI BgD Trans. Adv. Res.* **16** (2013) (<http://ipsitransactions.org/journals/papers/tar/2013jan/p4.pdf>)
11. S. S. Kocha, K. Shinozaki, J. W. Zack, D. J. Myers, N. N. Kariuki, T. Nowicki, V. Stamenkovic, Y. Kang, D. Li, D. Papageorgopoulos, *Electrocatal.* **8** (2017) 366 (<https://doi.org/10.1007/s12678-017-0378-6>)
12. A. N. Frumkin, *Z. Phys. Chem.* A164 (1933) 121
13. D. Strmcnik, K. Kodama, D. van der Vliet, J. Greeley, V. R. Stamenkovic, N. M. Marković, *Nature Chem.* **1** (2009) 466 (<https://doi.org/10.1038/nchem.330>)
14. B. Garlyyev, S. Xue, M. D. Pohl, D. Reinisch, A. S. Bandarenka, *ACS Omega* **3** (2018) 15325 (<https://doi.org/10.1021/acsomega.8b00298>)
15. S. Xue, B. Garlyyev, S. Watzele, Y. Liang, J. Fichtner, M. D. Pohl, A. S. Bandarenka, *ChemElectroChem* **5** (2018) 2326 (<https://doi.org/10.1002/celc.201800690>)
16. D. Karačić, S. Korać, A. S. Dobrota, I. A. Pašti, N. V. Skorodumova, S. J. Gutić, *Electrochim. Acta* **297** (2019) 112 (<https://doi.org/10.1016/j.electacta.2018.11.173>)
17. N. Gavrilov, I. A. Pašti, M. Mitić, J. Travas-Sejdić, G. Ćirić-Marjanović, S. V. Mentus, *J. Power Sources* **220** (2012) 306 (<https://doi.org/10.1016/j.jpowsour.2012.07.119>)

18. N. Gavrilov, I. A. Pašti, M. Vujković, J. Travas-Sejdic, G. Ćirić-Marjanović, S. V. Mentus, *Carbon* **50** (2012) 3915 (<https://doi.org/10.1016/j.carbon.2012.04.045>)
19. J.P. Perdew, K. Burke, M. Ernzerhof, *Phys. Rev. Lett.* **77** (1996) 3865 (<https://doi.org/10.1103/PhysRevLett.77.3865>)
20. P. Giannozzi, S. Baroni, N. Bonini, M. Calandra, R. Car, C. Cavazzoni, D. Ceresoli, G.L. Chiarotti, M. Cococcioni, I. Dabo, A.D. Corso, S. Fabris, G. Fratesi, S. de Gironcoli, R. Gebauer, U. Gerstmann, C. Gougoussis, A. Kokalj, M. Lazzeri, L. Martin-Samos, N. Marzari, F. Mauri, R. Mazzarello, S. Paolini, A. Pasquarello, L. Paulatto, C. Sbraccia, S. Scandolo, G. Sclauzero, A.P. Seitsonen, A. Smogunov, P. Umari, R.M. Wentzcovitch, *J. Phys.: Condens. Matter* **21** (39) (2009) 395502 (<http://dx.doi.org/10.1088/0953-8984/21/39/395502>)
21. A.S. Dobrota, I.A. Pašti, S. V. Mentus, N. V. Skorodumova, *Phys. Chem. Chem. Phys.* **19** (2017) 8530 (<https://doi.org/10.1039/c7cp00344g>)
22. N. P. Diklić, A. S. Dobrota, I. A. Pašti, S. V. Mentus, B. Johansson, N. V. Skorodumova, *Electrochim. Acta* **297** (2019) 523 (<https://doi.org/10.1016/j.electacta.2018.11.108>)
23. H.J. Monkhorst, J.D. Pack, *Phys. Rev. B* **13** (1976) 5188 (<https://doi.org/10.1103/PhysRevB.13.5188>)
24. S. Grimme, *J. Comput. Chem.* **27** (2006) 1787 (<https://doi.org/10.1002/jcc.20495>)
25. A.S. Dobrota, S. Gutić, A. Kalijadis, M. Baljozović, S. V. Mentus, N. V. Skorodumova, I.A. Pašti, *RSC Adv.* **6** (2016) 57910 (<http://dx.doi.org/10.1039/C6RA13509A>)
26. A.J. Bard, L.R. Faulkner, *Electrochemical Methods Fundamentals and Applications*, 2nd ed., John Wiley & Sons, Inc., New York, 2001.
27. D. W. H. Rankin, *CRC handbook of chemistry and physics*, 89th ed., David R. Lide, Ed., Taylor & Francis, Abingdon-on-Thames, 2008.
28. R. E. Davis, G. L. Horvath, C. W. Tobias, *Electrochim. Acta* **12** (1967) 287 ([https://doi.org/10.1016/0013-4686\(67\)80007-0](https://doi.org/10.1016/0013-4686(67)80007-0))
29. G. Ćirić-Marjanović, I. Pašti, S. Mentus, *Progress Mater. Sci.* **69** (2015) 61 (<https://doi.org/10.1016/j.pmatsci.2014.08.002>)
30. D. Hulicova, M. Kodama, H. Hatori, *Chem. Mater.* **18** (2006) 2318 (<https://doi.org/10.1021/cm060146i>).